Binns, R.A., Barriga, F.J.A.S., Miller, D.J., et al., 2002
Proceedings of the Ocean Drilling Program, Initial Reports Volume 193

6. SITE 1191[1]

Shipboard Scientific Party[2]

INTRODUCTION

Principal Results

Hole 1191A is located among chimneys in the Satanic Mills high-temperature hydrothermal site (see Fig. **F1,** p. 31, in the "Leg 193 Summary" chapter) and was cored during time made available while preparation for deployment of a casing string was under way. Drilling attained a depth of only 20.1 meters below seafloor (mbsf) because of borehole instability.

We drilled within the hard crust of vesicular dacite/rhyodacite found at the previous sites without passing through it. Drilling intersected fresh to mildly altered dacite-rhyodacite (70 wt% SiO_2 on an anhydrous basis) for the entire hole depth to 20.1 mbsf. This is moderately vesicular and aphyric in hand specimen. Large vesicles, as long as 4 cm, are severely stretched.

Alteration increases gradually downward, from slight to moderate. It consists of both replacement of the vitreous matrix and vesicle and fracture fillings. The igneous groundmass is replaced in patches by cristobalite and clay. Vesicles become lined by a silica + sulfide + clay coating, in which, for most vesicles, euhedral zeolites grow (possibly clinoptilolite and, much less abundant, phillipsite). Below ~11 mbsf, fractures and nearby vesicles are lined by subhedral marcasite, which includes framboids of pyrite. One marcasite veinlet has a selvage of more intense cristobalite-clay alteration. This alteration style differs from that found below fresh dacites at the top of previous holes drilled through hydrothermally active sites (Sites 1188 and 1189) in two main aspects: the absence of anhydrite (abundant at Sites 1188 and 1189) and the presence of abundant zeolites. This alteration style is believed to reflect passage of hydrothermal fluids almost to the seafloor.

[1]Examples of how to reference the whole or part of this volume.
[2]Shipboard Scientific Party addresses.

Ms 193IR-106

High-temperature hydrothermal chimneys surround Site 1191; thus, the alteration found may be considered weak. The absence of anhydrite may be explained by a variety of causes, including (1) alteration at temperatures below 150°C, (2) noninvolvement of unmodified seawater in the alteration, and (3) later dissolution by circulation of cooler fluid. The zeolites may have formed separately, perhaps during a cooling, oxidative episode after eruption of the lava.

One of the main results of Site 1191, coupled with the other sites, was to establish the general presence of the hard crust of fresh to weakly altered dacite/rhyodacite throughout Pual Ridge. Site 1191 samples provided a reliable estimation of the magnetic inclination (–16°), which is significantly different from the present-day value of ~7.7° for the region. Whereas this may result from a slight deviation during drilling with the rotary coring system, the more or less consistent magnetic inclination among sites and the young age of Pual Ridge suggests the presence of a tilted block.

Active bacterial cells were found by direct counting on two samples from depths of ~10 and 15 mbsf, respectively. Anaerobic bacterial cultivation tests on both samples yielded positive results at temperatures as high as 90°C.

Site Objectives

The main objective of drilling at this high-temperature venting site was to test for similarity or otherwise of its subsurface characteristics without more extensive characterization of the Roman Ruins hydrothermal site (Site 1189). Limited penetration resulted in only recovering the uppermost part of the lithologic section at Site 1191. However, as little time was effectively consumed drilling here (profiting from a necessity for other drill-rig operations), we consider the exercise as rather valuable, as it provided both additional fresh volcanic samples and a small-scale example of near-seabed hydrothermal activity.

Operations Summary

Hole 1191A

After operations at Hole 1188B, we chose to use the time while the drilling team was preparing for our casing deployment to attempt a single bit hole at one of our alternate high-temperature sites. During a 1.25-hr camera survey of the seafloor, we located a suitable position for Site 1191 (Table T1). We initiated Hole 1191A at 2045 hr on 27 November 2000, with the bit tagging the seafloor at 1705 meters below rig floor (mbrf) in an area of small standing and fallen chimneys. The vibration-isolated television sleeve was recovered, and continuous rotary core barrel coring continued through Core 193-1191A-3R to a depth of 1725.1 mbrf (20.1 mbsf). At that point, the driller lost rotation of the drill string. The pipe stuck with the bit only 17 mbsf. After working for 1.25 hr, the driller freed the pipe with 170 klb of overpull. However, upon deploying the next core barrel, the driller noted that the pump pressure was low, indicating that something might be keeping the barrel from landing and seating properly. Following two deployments of a bit deplugger, an inspection of the latch and landing shoulder assembly indicated that the barrel was indeed landing and latching properly. Pump pressures were normal with the bit off bottom, but lower than expected with the bit in contact with the bottom of the hole. After 10 hr

T1. Coring summary, p. 34.

of attempting to ream through 3 m of hard fill, we finally regained our original depth of 20.1 mbsf.

However, when we could not advance while cutting Core 193-1191A-4R even after 3 hr of rotation, we decided to terminate coring and move on to our casing attempt at Site 1188. On our ensuing wireline run, we were not able to engage the core barrel, so we tripped the pipe. The end of the drill string arrived on deck without the bit, the bit disconnect assembly, or the core barrel; apparently, the mechanical bit release had failed because of excessive wear during coring. Unfortunately, we had also deployed and lost the Lamont-Doherty Earth Observatory drill string accelerometer tool housing on our final coring attempt, and because it was unique, we did not have the opportunity for more temperature measurements using this tool. A total of 3.36 m of core was recovered for an overall average of 16.7% of the section cored (Table T1).

Site Survey

Targeted at the western side of the Satanic Mills hydrothermal site, the bit descended over rough volcanic outcrops. After we dropped a beacon, the bit was moved 20 m east across volcanic talus then descended 3 m to an area of chimney debris. Continuing 15 m farther (descending another 2 m), we passed a large (10 m) fallen chimney and several clusters of small standing chimneys venting shimmering fluid, before moving southwest for 10 m and spudding on fine chimney debris.

IGNEOUS PETROLOGY

Hole 1191A is situated in the Satanic Mills hydrothermal site between the Snowcap (Site 1188) and Roman Ruins (Site 1189) hydrothermal sites. Drilling intersected fresh to moderately altered, moderately vesicular, aphyric rhyodacite down to a depth of ~15 mbsf. Fresh, black rhyodacite (Fig. F1) occupies the uppermost part of Section 193-1191A-1R-1, and the refractive index (RI) measurements indicate an SiO_2 content of ~71 wt%. Alteration intensity increases from slight to moderate downhole and is marked by patchy to pervasive replacement of the black glassy to microcrystalline groundmass by silica and clay leading to a grayish, spotty appearance (Fig. F2). Zeolites (mainly clinoptilolite) are common within the vesicles and form radiating clusters on the inner vesicle walls. Below a depth of ~11 mbsf, several sulfide-rich hairline veins cut across the altered rhyodacite.

All the recovered volcanic rocks from Site 1191 have been logged as one unit because there is no change in primary lithologic features and alteration intensity increases gradually (Table T2). Therefore, we inferred that the rhyodacite was homogeneous in composition prior to alteration.

Volcanic Features

Primary volcanic features recognized in the Site 1191 specimens include vesicles, minor phenocrysts, and quenched or variably altered groundmass.

F1. Fresh and slightly altered, aphyric rhyodacite from the top of Hole 1191A, p. 14.

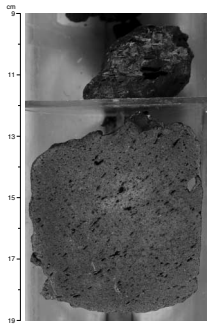

F2. Altered rhyodacite with spotty appearance and strongly elongated, tabular vesicle lined with fine zeolite crystals, p. 15.

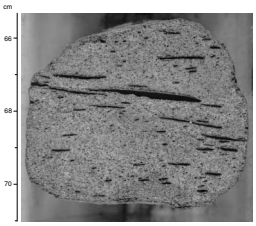

T2. Lithology and alteration of Unit 1, p. 35.

Vesicles

Round to elongate or tabular vesicles constitute 8–15 vol% of the recovered rocks. They show a wide range of dimensions from a fraction of a millimeter to several centimeters. Commonly, large vesicles as long as ~4 cm define a stretching direction parallel to the flow direction of the lava (Fig. F2). In some cases, the orientation of the stretching direction is normal to the long axis of core, indicating that flow was parallel to the current seafloor surface. In several other cases of oriented pieces, however, the flow directions indicated by stretched vesicles dip steeply (from ~45° to 90°).

Phenocrysts

The rocks have been classified as aphyric, based on hand specimen observation. However, thin-section examination shows that they contain scant plagioclase, clinopyroxene, and magnetite microphenocrysts, accounting for a trace to 0.4 vol% (Table T3). Plagioclase laths reach a maximum length of 1.2 mm, and stubby prismatic clinopyroxene crystals measure as wide as 0.4 mm. Magnetite grains, possibly microphenocrysts, are typically 10–40 µm across.

T3. Results of point counts on volcanic rock thin sections, p. 36.

Groundmass

In thin section, the groundmass of unaltered rhyodacite in Hole 1191A is brown and consists of fine feldspar microcryst needles and volcanic glass in roughly equal proportions (Fig. F3). The microcrysts are typically aligned in a preferred orientation defining a flow lamination.

This volcanic groundmass is replaced during alteration by a very fine grained mixture of silica and clay. Samples of slightly to moderately altered rhyodacite show a progressive change in the composition of the groundmass. Slightly altered samples contain irregular, semiconnected domains of unaltered groundmass surrounded by altered groundmass, whereas more intensely altered samples only contain remnant, irregular isolated "islands" of unaltered groundmass (Fig. F4). Vesicles in these rocks have a halo of altered groundmass indicating that pervasive alteration proceeded outward from these primary cavities.

Locally, where pervasive alteration is advanced, the remnants of the original groundmass are preserved only in rare isolated domains. These domains may have angular outlines with sharp margins to the surrounding altered groundmass and may be misinterpreted as xenoliths on superficial examination (Fig. F5).

F3. Fresh rhyodacite with about equal proportions of volcanic glass and fine microcrystalline plagioclase needles, p. 16.

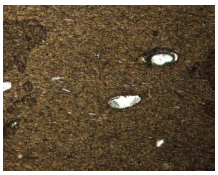

F4. Slightly altered rhyodacite with volcanic groundmass unevenly replaced by a very fine grained assemblage of silica and clay, p. 17.

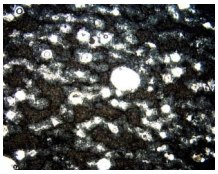

F5. Original groundmass locally preserved as isolated xenolith-like domains in moderately altered rhyodacite, p. 18.

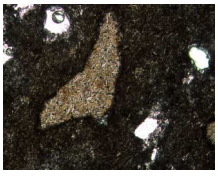

HYDROTHERMAL ALTERATION

Site 1191 is located at Satanic Mills, a site of high-temperature hydrothermal venting and sulfide chimney development located between the low-temperature Snowcap (Site 1188) and high-temperature Roman Ruins (Site 1189) hydrothermal sites. We therefore felt that Site 1191 would provide a good location to test whether a similar style of subsurface alteration to that observed at Snowcap and Roman Ruins hydrothermal sites could reasonably be assumed to underlie the bulk of the PACMANUS hydrothermal field. Unfortunately, drilling conditions proved difficult, and Hole 1191A was abandoned at a depth of only

20.1 mbsf without reaching the zone of pervasive hydrothermal alteration, meaning that this hypothesis remains untested.

The vesicular volcanic rocks that were recovered from Hole 1191A at Satanic Mills hydrothermal site were classified as a single lithologic unit, which ranges from fresh to moderately altered (Fig. F1) (see "Site 1191 Alteration Log," p. 14).

Intervals 193-1191A-1R-1, 0–11 cm (0.00–0.11 mbsf), and 3R-1, 9–26 cm (14.79–14.96 mbsf), are fresh, glassy, aphyric lavas. Alteration of these rocks is restricted to thin films of clayey material and occasional Fe-oxyhydroxide coatings on fracture surfaces. The deeper interval is possibly composed of pieces that have fallen from higher in the hole.

All other samples from Hole 1191A exhibit slight to moderate alteration manifested by patchy to pervasive replacement of the glassy portion of the igneous groundmass by cristobalite (from X-ray diffraction [XRD] analysis) (Table T4), clay, and disseminated marcasite and minor pyrite. Aggregates of framboidal pyrite were observed in a thin section of Sample 193-1191A-2R-2, 103–106 cm. Microlitic plagioclase and scattered phenocrysts of plagioclase, augite, and magnetite are unaffected by the alteration (Fig. F6).

The vesicles of slightly to moderately altered rocks from Site 1191 are lined with a soft, drusy material that contains microcrystalline silica, sulfide, and possibly a clay mineral. Most vesicles also contain rosettes of zeolite overgrowing the silica-clay. The most abundant zeolite in vesicles is colorless and platy, often forming rosette-like aggregates. The mineral has an RI of ~1.48 and a platy habit suggesting that it may be clinoptilolite. Clinoptilolite has also been tentatively described in thin sections, where it appears as vesicle fill in the form of blocky to platy colorless crystals with low birefringence. A much less abundant second zeolite has been observed to form rosettes of radiating, milky, acicular crystals in vesicles. The crystal habit indicates that this zeolite may be phillipsite.

A small number of core pieces show slight brown weathering (see "Site 1191 Alteration Log," p. 14), and vesicles near weathered surfaces contain black botryoidal spots that are possibly hematite or goethite. These samples also contain, in addition to the other zeolites, blocky clear crystals of a third zeolite, with an RI of 1.494, thought to be heulandite.

Sulfide veins (marcasite and minor pyrite), 2 mm wide, are found at the fractured ends of many individual core pieces. One interval (193-1191A-2R-1, 103–109 cm) is cut by a 1- to 2-mm-wide marcasite-pyrite vein along which a 1-cm-wide pale alteration halo is developed. The alteration style in the vein halo is similar to that in other parts of the core (silica-clay with disseminated sulfides), but the intensity of alteration is significantly higher.

T4. Minerals identified by XRD analysis, p. 37.

F6. Cristobalite-clay alteration of pale brown volcanic glass in a moderately altered volcanic rock, p. 19.

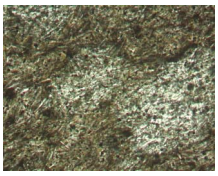

Discussion

Alteration of volcanic rocks at Site 1191 (Satanic Mills hydrothermal site) is limited to moderate intensity cristobalite-clay alteration of the glassy portion of the groundmass, with marcasite-(pyrite) veining and zeolite vesicle fill. This alteration differs from that seen in the upper portion of Hole 1189A (Roman Ruins hydrothermal site), where more intense cristobalite-clay alteration is associated with anhydrite-pyrite veining. However, given the generally low recovery at both locations, some caution must be exercised when comparing core from the two sites.

The increase in intensity of cristobalite-clay alteration in the halos of marcasite-pyrite veins at Site 1191 indicates a genetic link between the alteration and the veining. Consequently, cristobalite-clay alteration and sulfide veining are interpreted to have formed by interaction of the rocks with a hydrothermal fluid (rich in SiO_2, Fe, and H_2S). Spotty iron oxides and zeolites are confined to vesicles and fracture surfaces and are thought to represent later low-temperature, seawater-dominated oxidative alteration that may have no direct relationship to circulation of hydrothermal fluids.

Anhydrite, a common vein and vesicle fill in the uppermost portions of the hydrothermal system at Sites 1188 and 1189, has not been identified in rocks from Hole 1191A. The lack of anhydrite in the shallow subseafloor at Satanic Mills hydrothermal site may be caused by one or more of the following reasons:

1. The temperature of hydrothermal alteration at 15.65 mbsf may not have exceeded 150°C, thus inhibiting anhydrite precipitation.
2. There was insignificant subsurface mixing with seawater.
3. Previously precipitated anhydrite was dissolved during later low-temperature oxidative alteration, which postdates the hydrothermal alteration in Hole 1191A.

SULFIDE AND OXIDE PETROLOGY

Hole 1191A

In hand specimen, euhedral pyrite fills vesicles and forms thin (<0.5 mm) veins in slightly altered aphyric, moderately vesicular rhyodacite. Some of this "pyrite" identified with the hand lens may actually be marcasite (see next paragraph) but, unless known otherwise from thin section, is referred to as pyrite. The pyrite is brass colored where euhedral, and it is steel gray on broken surfaces. It is coated in places with a thin film of silica. Pyrite is also intergrown with silica and zeolites in vesicles or is precipitated on silica that lines vesicle walls. Commonly, the core was broken along the veins. Veins for which both walls are present are vuggy, with euhedral pyrite. Vesicles within a millimeter of a pyrite vein commonly contain pyrite and silica, and there is one example (Section 193-1191A-2R-2 [Piece 16]) of pyrite, marcasite, and silica in a 1-cm-wide halo of alteration on either side of a marcasite vein. This marcasite was identified in thin section (see next paragraph). Anhydrite is not observed in the veins or vesicles. Even though some veins contain close to 100% pyrite or marcasite, they are not sufficiently numerous to raise the sulfide content of the samples to the 5% required to be considered a sulfide rock.

Figure F7 shows that the euhedral vein marcasite (thought to be pyrite in hard specimen) in Section 193-1191A-2R-2 (Piece 16) has cores of framboids. The framboids are 0.01–0.05 mm in diameter and individual granules are 0.5–1 µm in diameter. The framboids look like pyrite, but pyrite framboids are typically associated with organic-rich sediments and form in the water column just above the seafloor at a redox boundary (Wilkin and Barnes, 1997). Therefore, these framboids are possibly made of the iron sulfide spinel, greigite (Fe_3S_4), which is indistinguishable from pyrite in thin section. It is also possible that greigite framboids recrystallized into pyrite, preserving the framboidal texture.

F7. Framboids of possible greigite or pyrite in a marcasite-filled vein, p. 20.

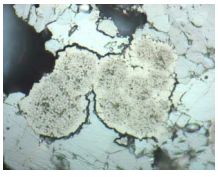

STRUCTURAL GEOLOGY

The structures identified in the core from Hole 1191A were primary volcanic layering, elongation of vesicles, and silica-pyrite veins. These were described on the structural visual core descriptions (see **"Site 1191 Visual Core Descriptions,"** p. 1) and recorded in the structural log (see **"Site 1191 Structural Log,"** p. 16).

Orientation of Primary Layering

In the volcanic rocks found throughout the recovered core, the original layering was identified from the orientation of elongate flattened and stretched vesicles in some of the massive lavas, and in other parts of the core, from millimeter-scale color banding attributed to flow. The individual flow bands consist of differences in the amount and size of the microlites formed during crystallization and by the different degrees of vesicularity. The vesicles were found commonly to display a stretching lineation. The stretching and flattening of vesicles most probably formed during flow of viscous lava, and thereby they define the direction of flow.

The lineations show shallow plunges, between 4° and 21°, except for one measurement of 38°, whereas the layering defined by the arrays of vesicles has dips of between 7° and 88° (Fig. **F8A**). In the upper meter of the hole, the dip of the layering changes from ~45° at 0.12 mbsf to subhorizontal at 0.52 mbsf. Most of the measurements are from Sections 193-1191A-2R-1 and 2, between 9.51 and 12.03 mbsf. In this interval, the dip of layering has a trend from subvertical at 9.51 mbsf, gradually decreasing downward to a dip of ~40° at 12 mbsf. In Section 193-1191A-3R-1, the measurements indicate a steepening trend of the dips of layering from ~40° at 15.21 mbsf to ~60° at 15.56 mbsf. The plunges of the lineations, however, as mentioned above, are generally <20°. If the variations in the dips of layering were caused by the intersections of different rotated lava blocks, a change in orientation of the plunges of lineations would also be expected. Because this is not the case, the most likely explanation for the variations in dips of layering is folding. The folding would have happened during the flow of the viscous lava.

In six cases in the hole between 9.51 and 15.21 mbsf, it was possible to measure both the direction of stretching and layering in the same pieces (Fig. **F8B**). These measurements show that although the layering as defined by the trails of the flattened vesicles is generally steep, the flow direction of the lava, as defined by the direction of vesicle elongation lineation, is close to horizontal. This could mean that Hole 1191A intersected the outer parts of a lava flow in this interval, as depicted in Figure **F8C**.

F8. Variation in dips and plunges and the relationships between volcanic layering and lineations, p. 21.

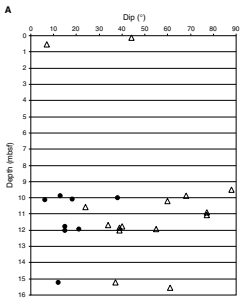

Vein Geometry and Mineralogy

Only 16 veins, commonly forming the broken ends and surfaces of the core pieces, were intersected in Sections 193-1191A-2R-1 and 2R-2, between 10 and 12 mbsf. With but one exception, these veins are dominated by fine-grained pyrite and/or marcasite with minor silica. The exception was a <0.2-mm-thick vein consisting solely of silica. The veins are all very thin, mostly <1 mm in thickness, only one vein being 1–1.5 mm thick.

With respect to dips of the veins, one is nearly horizontal and one is vertical, whereas the others dip between 19° and 59° (Figure F9).

The thickest vein, with a dip of 52°, was the only one that was examined under the microscope (Sample 193-1191A-2R-2 [Piece 16, 103–106 cm]). This vein is 1–1.5 mm thick and consists of framboidal pyrite or greigite(?) overgrown by marcasite (see "Sulfide Petrology," p. 6). Fine-grained silica, probably cristobalite, is present in trace amounts between the sulfide grains. A faint, <0.3-mm-thick halo of silica-clay is present beside the vein. Disseminated marcasite, partly with cores of framboids, similar to the assemblage in the vein, extends for 2–3 mm out from both sides of the vein, posing questions regarding conventional models for the origin of framboids.

F9. Variation of dip vs. depth of pyrite-silica veins, p. 23.

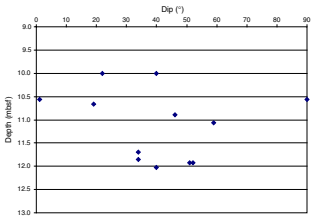

GEOCHEMISTRY

Five representative igneous rocks were analyzed from Hole 1191A. The analytical methods included elemental analyses of total hydrogen and sulfur by NCS (nitrogen, carbon, sulfur) elemental analysis, and the inductively coupled plasma–atomic emission spectroscopy (ICP-AES) for the major element oxides and the trace elements (Zr, Sr, Cu, Zn, Ba, and Y).

Results

Analyses of ignited samples from Hole 1191A and the calculated whole rock compositions are listed in Table T5. The ignited sample results are recalculated with respect to loss on ignition and are used for the compositional diagrams in Figures F10 and F11. The compositions of the samples from Hole 1191A are all similar and compare closely with the composition of the fresh rock samples in two previous holes (Samples 193-1188A-2R-1, and 193-1190C-2R-1) but are richer in SiO_2 than 193-1189A-IR-1. In Figures F10 and F11, these three samples are plotted along with the five samples from Hole 1191A. The rocks from Hole 1191A may be classified as dacites both using the total alkalis vs. silica plot (Fig. F10) or using the IUGS (CIPW norm) classification (Fig. F11). In both figures, the sample from Hole 1189A (Sample 193-1189A-1R-1, 0–4 cm) is distinctive on account of its lower silica content relative to the other seven samples, which trend toward rhyodacite compositions (see "Geochemistry," p. 15, in the "Explanatory Notes" chapter).

T5. Major element and selected trace element compositions, p. 38.

F10. Chemical classification of fresh volcanic rocks, p. 24.

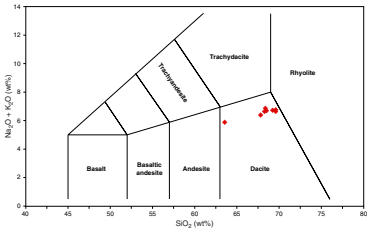

F11. IUGS classification of fresh volcanic rocks, p. 25.

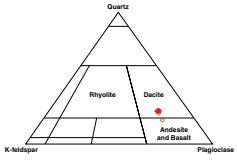

MICROBIOLOGY

Two samples were collected prior to curation from Hole 1191A for shipboard studies (direct microscopic enumeration, adenosine triphosphate [ATP] analysis, micromorphological descriptions, and enrichment cultures). Corresponding samples were collected for shore-based studies (aerobic and anaerobic culturing, biochemical and molecular typing, and microscopic determination of the role of microbes in mineralization and alteration).

Total Bacterial Enumeration and ATP Analysis

Following methods described in "Microbiology," p. 19, in the "Explanatory Notes" chapter, samples were stained with 4,6-diamindino-2-phenylindole (DAPI), and the direct bacterial counts are shown in Table T6. Bacteria were found in both samples. The bacterial mass decreased from 1.4×10^7 cells/cm^3 in Sample 193-1191A-2R-1, 115–130 cm (10.55 mbsf), to 5.8×10^6 cells/cm^3 in Sample 193-1191A-3R-1, 62–65 cm (15.32 mbsf). ATP was detected in both samples, the amounts being approximately the same in both samples (Table T6), therefore, indicating similar biomass activities at these depths. The detection limits of total bacterial counts and ATP analysis are 1.0×10^5 cells/cm^3 and 0.5 pg/cm^3, respectively. These results show that a large and active bacterial population exists to the bottom of the hole at a depth of 15 mbsf.

T6. Total bacterial counts and ATP measurements, p. 39.

Enrichment Cultivation

Enrichment cultivation of microbes was conducted to improve the yield of microorganisms in the core samples. The cultivation cultures were conducted at varying temperatures and oxygen partial pressures (Table T7). Bacterial growth was routinely determined by comparing inoculated cultures with the uninoculated medium, where turbidity indicates bacterial growth. In cultures where it was difficult to make an assessment based on a visual observation, ATP analysis was conducted to confirm growth. Results of these experiments (after 1 week of incubation) are shown in Table T7. In the aerobic cultures, growth was observed at 4°C (Sample 193-1191A-2R-1, 115–130 cm [10.55 mbsf]) and 25°C (Samples 193-1191A-2R-1, 115–130 cm [10.55 mbsf], and 3R-1, 62–65 cm [15.32 mbsf]). No growth was observed with any of the samples at 60°C. In the anaerobic cultures, growth was observed in both samples at all the incubation temperatures. These observations suggest that a large diversity of aerobic and anaerobic (thermophilic, extreme thermophilic, and hyperthermophilic) bacteria exist to 15 mbsf and are, therefore, consistent with the direct count and ATP results.

T7. Enrichment cultivation at different cultivation conditions, p. 40.

Micromorphological Observations

Optical and epifluorescence microscopic techniques were used to characterize the interactions between microorganisms and minerals, in particular the micromorphology, size, chemical composition, and structure of minerals associated with the microorganisms. These observations are essential for establishing the biological habitat and the role of microbes in the mineralization and alteration processes in this hydrothermal system.

Samples 193-1191A-2R-1, 115–130 cm (10.55 mbsf), and 3R-1, 62–65 cm (15.32 mbsf), consist mainly of transparent and translucent fragments of dacitic volcanic glass with embedded magnetite (Fig. F12A). Some fragments contained spherical opaque grains of magnetite embedded in glass (Fig. F12B) and lath-shaped plagioclase microlites (Fig. F12B). Sparse bacterial populations were located on the surface of these fragments, including a few bacterial colonies (Fig. F12C).

F12. Dacitic volcanic glass with embedded magnetite and plagioclase microlites showing bacterial habitation, p. 26.

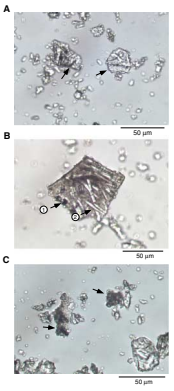

PHYSICAL PROPERTIES

Physical properties measurements taken on core recovered from Site 1191 (Satanic Mills hydrothermal site) include magnetic susceptibility, natural gamma radiation, compressional wave velocity, thermal conductivity, and standard index properties. The magnetic susceptibility meter and natural gamma radiation device were run on all cores (Cores 193-1191A-1R through 3R) recovered from Hole 1191A using the multisensor track. Where possible, compressional wave velocity measurements were made in only one direction on discrete samples. Thermal conductivity was measured throughout the one lithologic unit recovered from this hole. Index properties were measured on three discrete minicore samples.

Magnetic Susceptibility

Figure F13 shows the downhole profile for magnetic susceptibility from the seafloor to 16 mbsf. The values range from 32.1 × 10^{-5} to 1168.1 × 10^{-5} SI, with an average of 416 × 10^{-5} SI. The magnetic susceptibility is high throughout the core, with the highest values concentrated in Core 193-1191A-2R. Although only small amounts of magnetite were observed in thin section, very fine grains of magnetically susceptible material may be in the groundmass, which could account for the high values.

Natural Gamma Radiation

Natural gamma radiation (NGR) records are summarized in plots of total counts per second (cps) vs. depth (see Fig. F14). NGR values range from 3.1 to 16.2 cps, averaging 10 cps. As with Sites 1188 and 1189, much of the variation may be caused by errors in the measurement process (see "Physical Properties," p. 74, in the "Site 1188" chapter). The values from this site are on average similar to those of fresh volcanic rocks from the top of Hole 1188A, but are significantly lower than those of fresh, less siliceous, volcanic rocks from the top of Hole 1189A.

Compressional Wave Velocity

Two compressional wave velocity values were obtained from Hole 1191A. Data for these samples are shown in Table T8. Both samples, taken from unaltered dacites that are moderately vesicular, have velocities >5 km/s.

Thermal Conductivity

Thermal conductivity measurements for the recovered core span a small range of values, from 1.25 to 1.79 W/(m·K) (Fig. F15). The average value of the measurements, 1.45 W/(m·K), is consistent with measurements from unaltered dacites from Holes 1188A and 1189A.

Index Properties

The data for water content, bulk density, dry density, grain density, porosity, and void ratio are displayed in Table T9. Grain densities measured on ICP-AES powder samples are given in Table T10. There is very

F13. Magnetic susceptibility, p. 27.

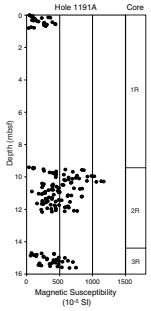

F14. Natural gamma radiation, p. 28.

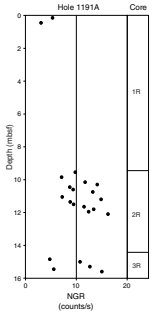

T8. Compressional wave velocities, p. 41.

F15. Thermal conductivity, p. 29.

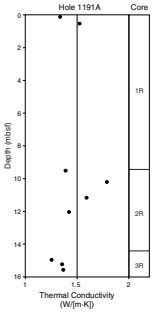

T9. Index properties, p. 42.

T10. ICP powder grain densities, p. 43.

little variation in the grain density values of the minicore samples, which range from 2.5 to 2.6 g/cm^3. These values are generally consistent with those from other unaltered dacites at Sites 1189 and 1190. They are also generally similar to ICP-AES grain densities, but because ICP-AES samples and minicore samples were taken from different intervals, exact comparisons cannot be made. The porosity values also differ very little, with values ranging from 7.1% to 11.5%.

ROCK MAGNETISM

Site 1191 was drilled to only 20.1 mbsf and, therefore, did not help clarify the deep magnetic structure at Pual Ridge. However, by virtue of reasonable recovery of continuous core pieces, this site provides important information regarding the magnetic properties of the near-seabed cap of relatively unaltered dacite lava. The results of our analyses show that Site 1191 has a relatively high remanent intensity compared to samples from other sites at similar depths. However, the susceptibility appears to be substantially to slightly less than that of other sites. Hole 1191A also provides interesting information on magnetic inclination.

Remanence and Susceptibility Measurements

The recovery was low in Hole 1191A, and all of the cores had significant gaps between pieces. In many cases, the recovered material was not cylindrical; thus, the split cores often did not fill the core liners. We took susceptibility and remanence measurements of the archive-half cores at places where rock pieces were long enough. Susceptibility measurements of the archive-half cores were taken by setting the point susceptibility meter on the archive multisensor track in manual mode and placing the probe in contact with the piece of core. Figure **F16** shows a downhole profile of the susceptibility measurements of the archive-half cores and the minicores. The susceptibility values range from 0.005 to 0.013 SI units, and results for both sample types are consistent.

Three minicore samples were taken from Hole 1191A. Table **T11** summarizes the magnetic properties of these samples. We also measured the anisotropy of magnetic susceptibility (AMS) of the minicores. Table **T12** summarizes the magnitudes and principal axes of the AMS that were derived from the susceptibility tensor. Figure **F17** is a Flinn-type diagram representing the susceptibility ellipsoid in two-dimensional space. There appears to be very little anisotropy of the magnetic susceptibility of samples from Site 1191. The remanent intensities were measured by performing step-wise alternating-field (AF) demagnetization at peak fields of 10, 15, 20, 25, 30, 40, 50, 60, and 80 mT. The changes in the magnetization intensity, inclination, and declination measurements of the minicore samples are summarized in Table **T13.**

The natural remanent magnetization (NRM) intensity of the minicore samples ranges from 4.5 to 7.6 A/m, which is substantially higher than that of other sites at similar depths (Fig. **F18**). In the case of Site 1189, one minicore at 9.8 mbsf has an NRM intensity of 1.55 A/m (Fig. **F134,** p. 210, in the "Site 1189" chapter), and the maximum intensity of the archive-half cores is <3 A/m (Fig. **F131,** p. 207, in the "Site 1189" chapter). This contrasts with the susceptibility values, which are substantially lower than those of Sites 1188 (Fig. **F124,** p. 234, in the "Site 1188" chapter) and 1189 (Figs. **F130,** p. 206, and **F132,** p. 208, both in the "Site 1189" chapter). Consequently, the entire suite of minicore

F16. Volume susceptibility of archive-half–core and minicore samples, p. 30.

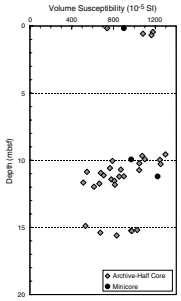

T11. Magnetic properties of minicores, p. 44.

T12. Anisotropy of magnetic susceptibility, p. 45.

F17. Anisotropy of magnetic susceptibility, p. 31.

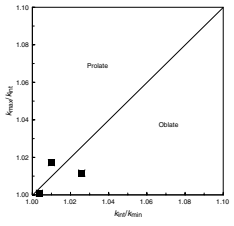

T13. Magnetic properties of minicores after alternating-field demagnetization, p. 46.

F18. Natural remanent magnetization intensity of archive-half–core and minicore samples, p. 32.

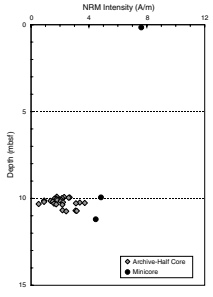

samples from Hole 1191A exhibit very high Koenigsberger ratios. The minicore samples provide valuable information on the magnetic inclination of the fresh volcanic cap to Pual Ridge at Site 1191 (Table T11). The inclination values are quite consistent between samples. The average value of –16° is slightly steeper than that of the present-day Earth field, but is the same as the average value that we obtained for Site 1188. According to the International Geomagnetic Reference Field for December 2000, this drill site has an inclination of –7.7°.

Thermal Demagnetization

We conducted a thermal demagnetization experiment on only one sample from Site 1191 because all the minicore samples appear to have similar characteristics. Figure F19 shows the thermal demagnetization curve of Sample 193-1191A-2R-2, 30 cm. The sample was first imparted with a saturated isothermal remanent magnetization at an impulse field of 1.1 T. After each step of heating, the sample was cooled back to room temperature and its intensity measured. The demagnetization curve shows a rise in intensity to ~300ºC followed by a steady drop to 600°C (Fig. F19). Based on this observation, it appears that the dominant magnetic mineral is magnetite, which has a Curie temperature of 585ºC (Table T27, p. 305, in the "Site 1188" chapter). There may be a slight amount of titanomagnetite since a large drop in intensity starts at ~350°C.

F19. Thermal demagnetization curve of a dacite sample, p. 33.

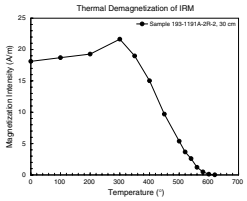

REFERENCE

Wilkin, R.T., and Barnes, H.L., 1997. Formation processes of framboidal pyrite. *Geochim. Cosmochim. Acta,* 61:323–339.

Figure F1. Photograph of fresh (interval 193-1191A-1R-1, 9.5–11.5 cm) to slightly altered (interval 193-1191A-1R-1, 12–18.5 cm) aphyric rhyodacite from the top part of Hole 1191A. The main stretching orientation of the vesicles is normal to the surface of the sample (interval 193-1191A-1R-1, 9–19 cm).

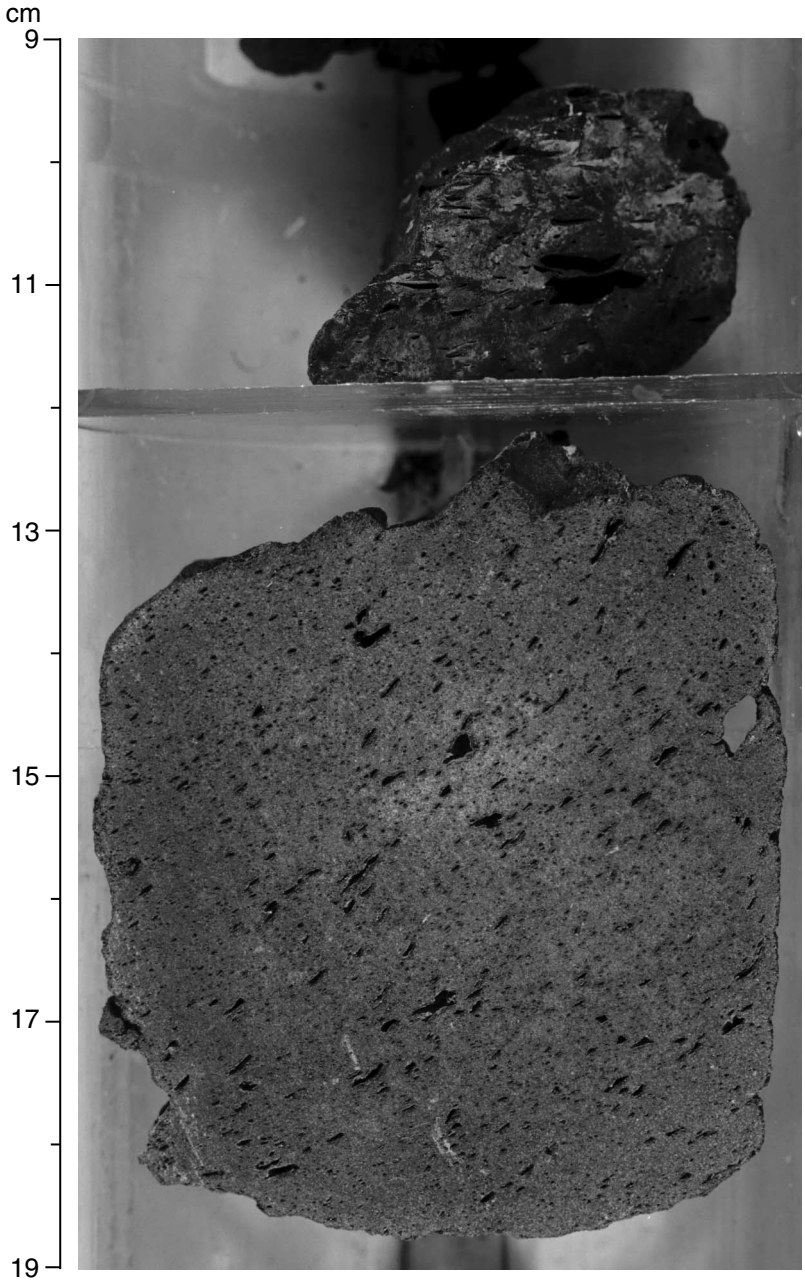

Figure F2. Photograph of altered rhyodacite with a spotty appearance and a strongly elongated tabular vesicle lined with fine zeolite crystals. The spotty appearance is caused by partial alteration of the volcanic groundmass forming very fine grained silica and clay minerals (interval 1191A-1R-1, 65.5–71.5 cm).

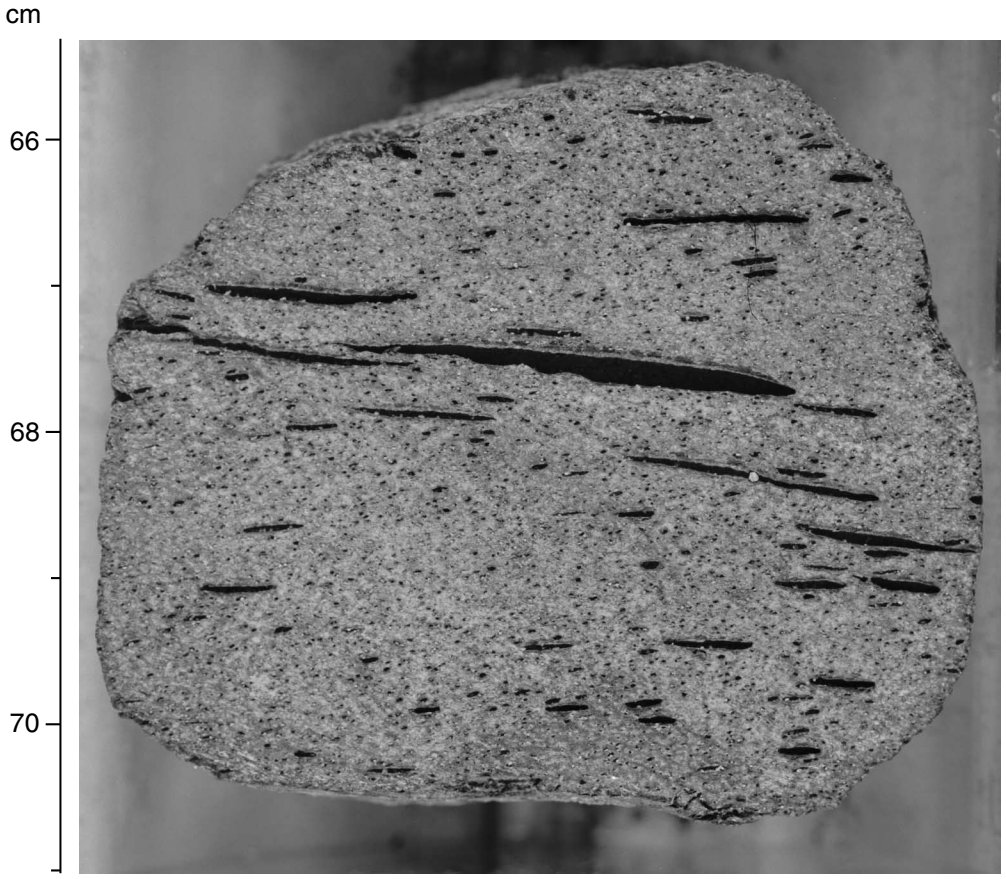

Figure F3. The groundmass of fresh rhyodacite in the uppermost part of Hole 1191A consists of about equal proportions of volcanic glass and fine microcrystalline plagioclase needles, which are generally aligned (Sample 193-1191A-1R-1 [Piece 2, 5–11 cm] in plane-polarized light; width of view = 1.38 mm. Photomicrograph ID# 1191A_1; **thin section 47**).

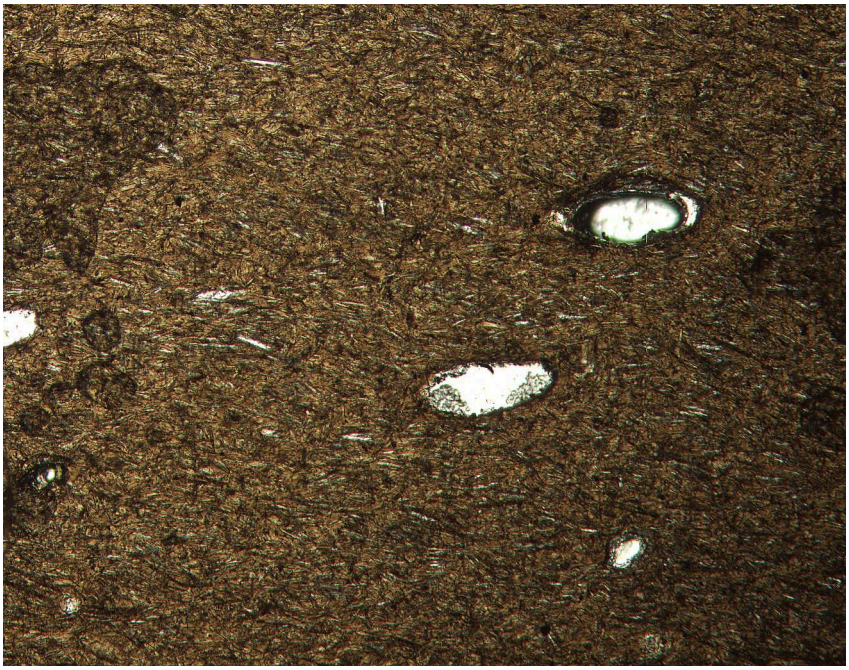

Figure F4. Slightly altered rhyodacite with volcanic groundmass that is unevenly altered to a very fine grained assemblage of silica and clay. (Sample 193-1191A-3R-1 [Piece 9, 51–54 cm] in plane-polarized light; width of view = 5.5 mm. Photomicrograph ID# 1191A_9; **thin section 52**).

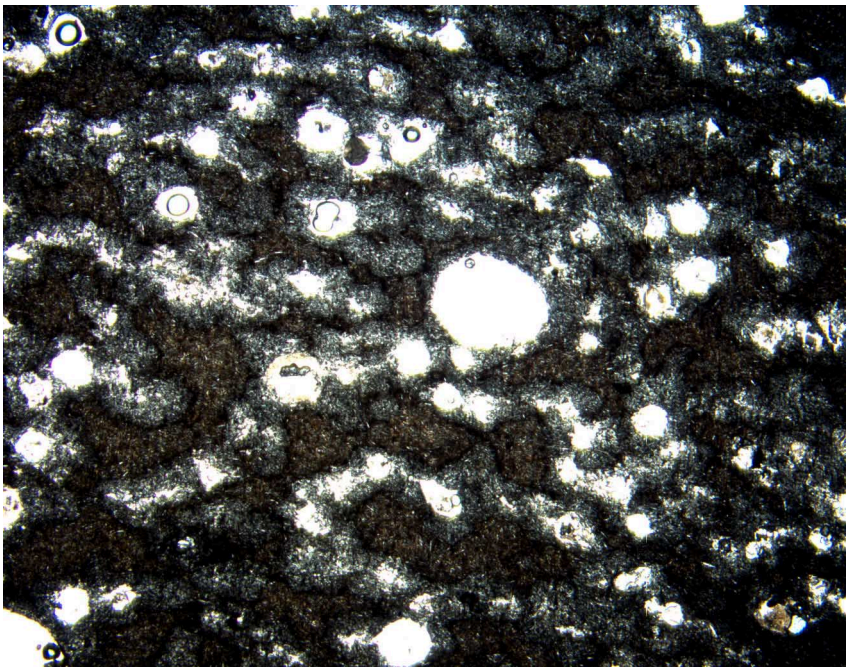

Figure F5. Moderately altered rhyodacite where remnants of the original groundmass are locally preserved as isolated xenolith-like domains with sharp, angular outlines in thin section (Sample 193-1191A-3R-1 [Piece 1, 0–9 cm] in plane-polarized light; width of view = 1.38 mm. Photomicrograph ID# 1191A_10; **thin section 50**).

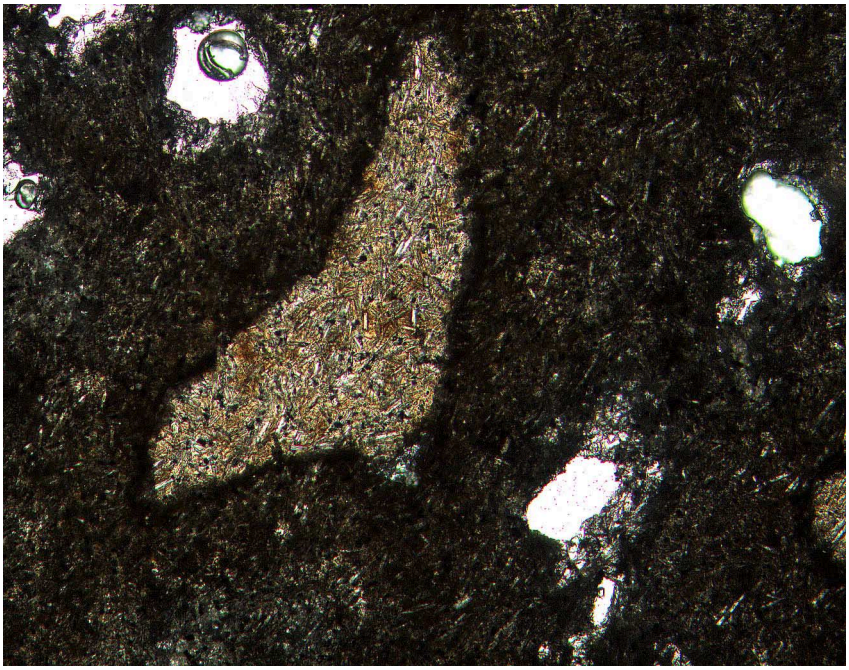

Figure F6. Photomicrograph illustrating cristobalite-clay alteration (colorless patches) of pale brown volcanic glass in a moderately altered volcanic rock from Site 1191. Note that microlitic plagioclase and magnetite (fine opaque spots) are apparently unaffected by the alteration (interval 193-1191A-2R-2, 103–106 cm, in plane-polarized light; field of view = 0.7 mm. Photomicrograph ID# 1191A_7; **thin section 49**).

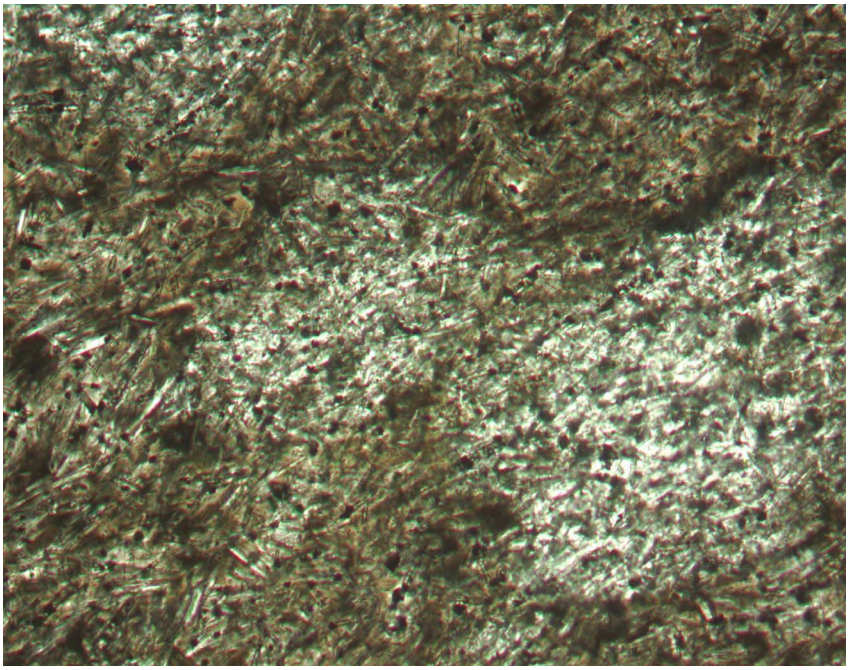

Figure F7. Oil-immersion photomicrograph in reflected light of framboids of pyrite (or possible greigite, Fe_3S_4) in a vein dominated by marcasite (Section 193-1191A-2R-2 [Piece 16, 103–106 cm]; width of view = 0.14 mm. Photomicrograph ID# 1191A_04, **thin section 49**).

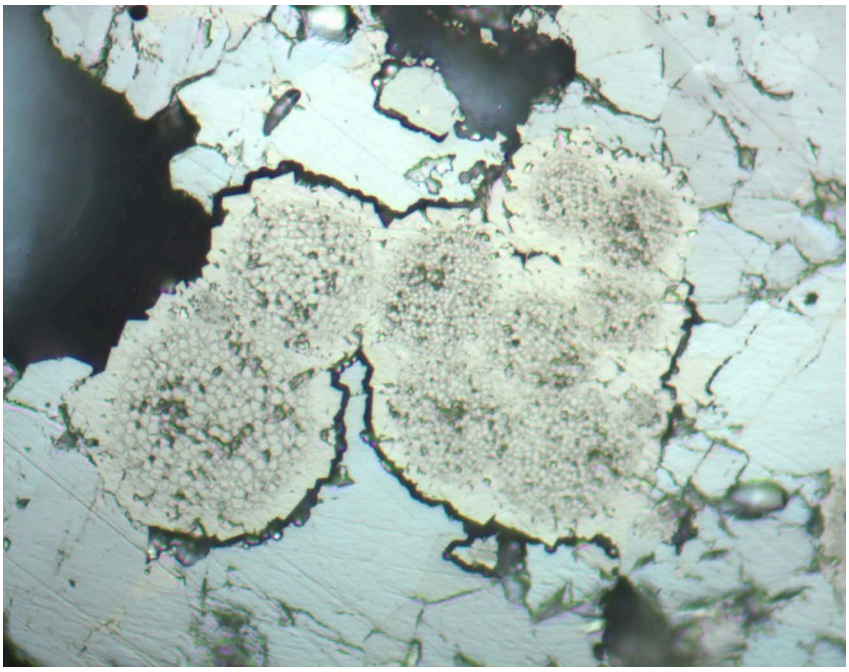

Figure F8. A. Variation in dips of volcanic layering (open triangles) and plunges of lineations defined by stretched vesicles (solid circles) in volcanic rocks with depth in Hole 1191A. (Continued on next page.)

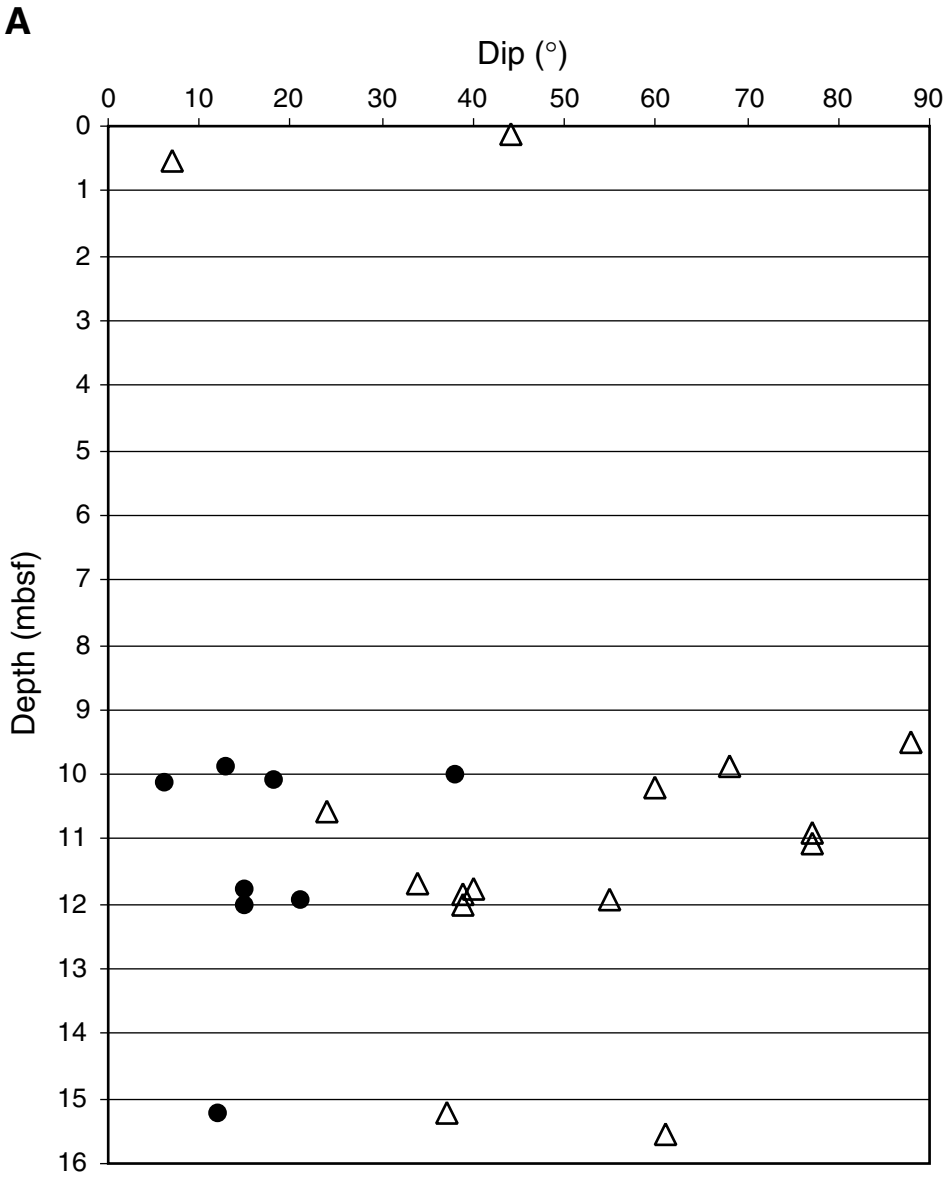

Figure F8 (continued). B. Relationships between volcanic layering (great circles) and lineations (solid circles) defined by stretched vesicles in cases where both were measured in the same core pieces in Hole 1191A. Arrows = the measurement pairs (Equal area, southern hemisphere projection). **C.** Sketch indicating the possible relationship between flow banding and the elongation of vesicles based upon the relationship shown in (B).

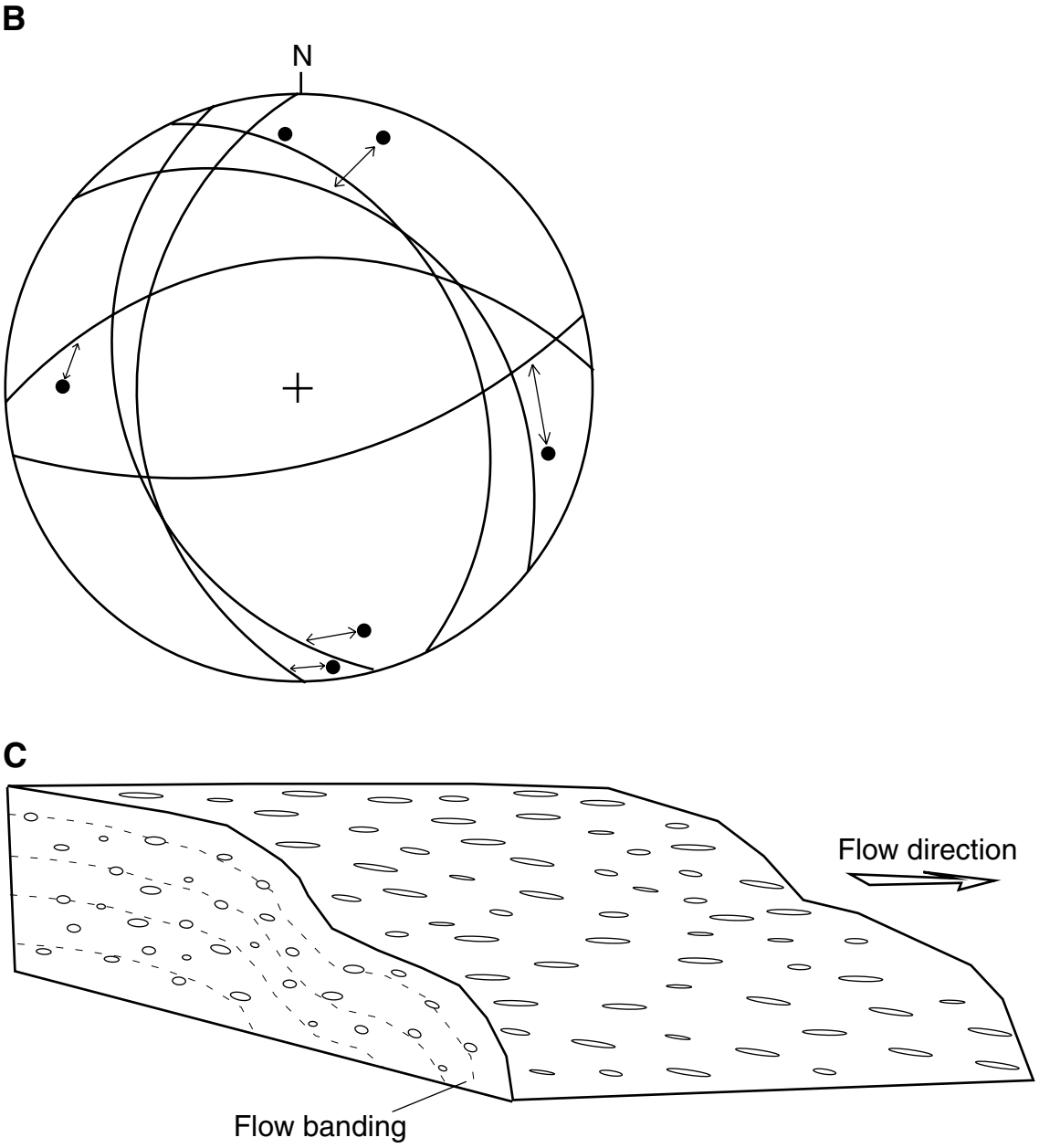

Figure F9. Variation of dip vs. depth of pyrite-silica veins, Hole 1191A.

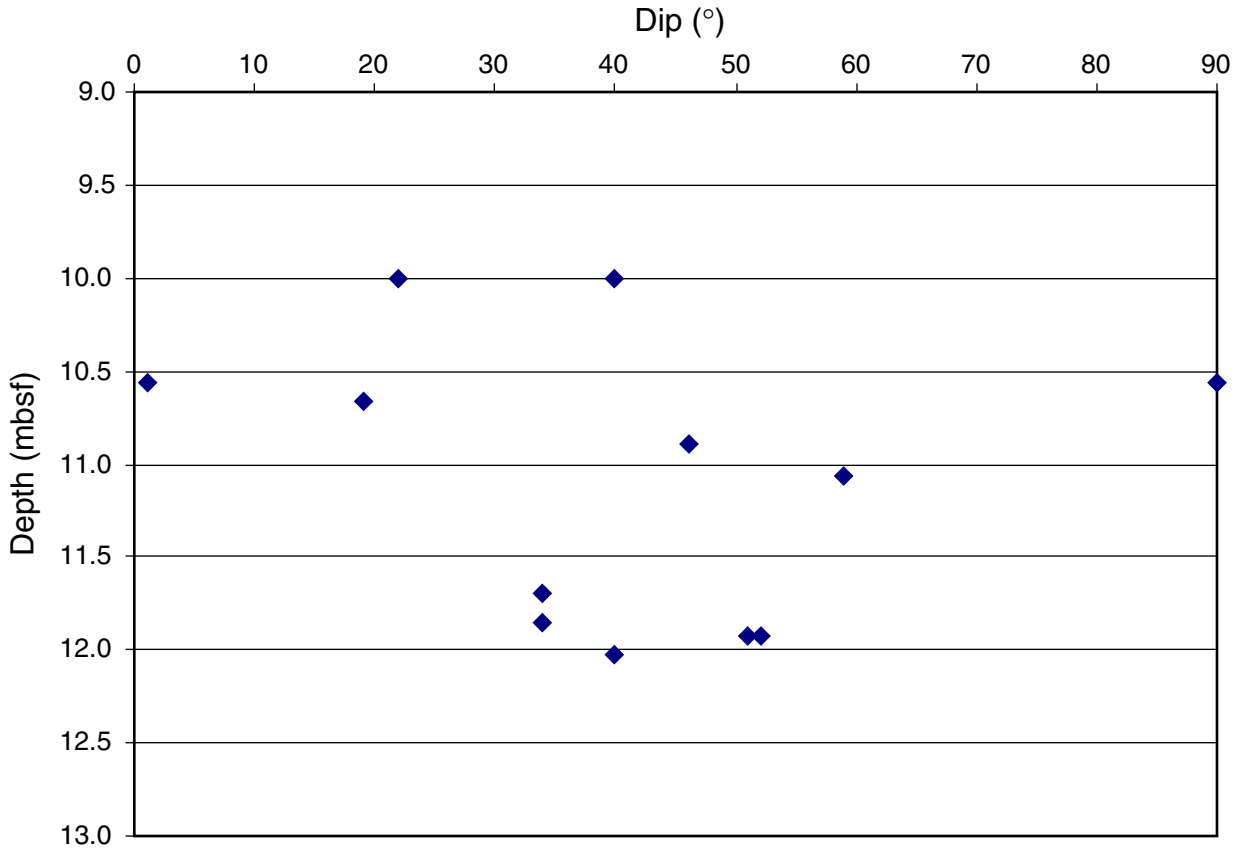

Figure F10. Chemical classification of fresh volcanic rocks from Hole 1191A, along with single samples for each of Holes 1188A, 1189A, and 1190C, using the total alkalis vs. silica diagram.

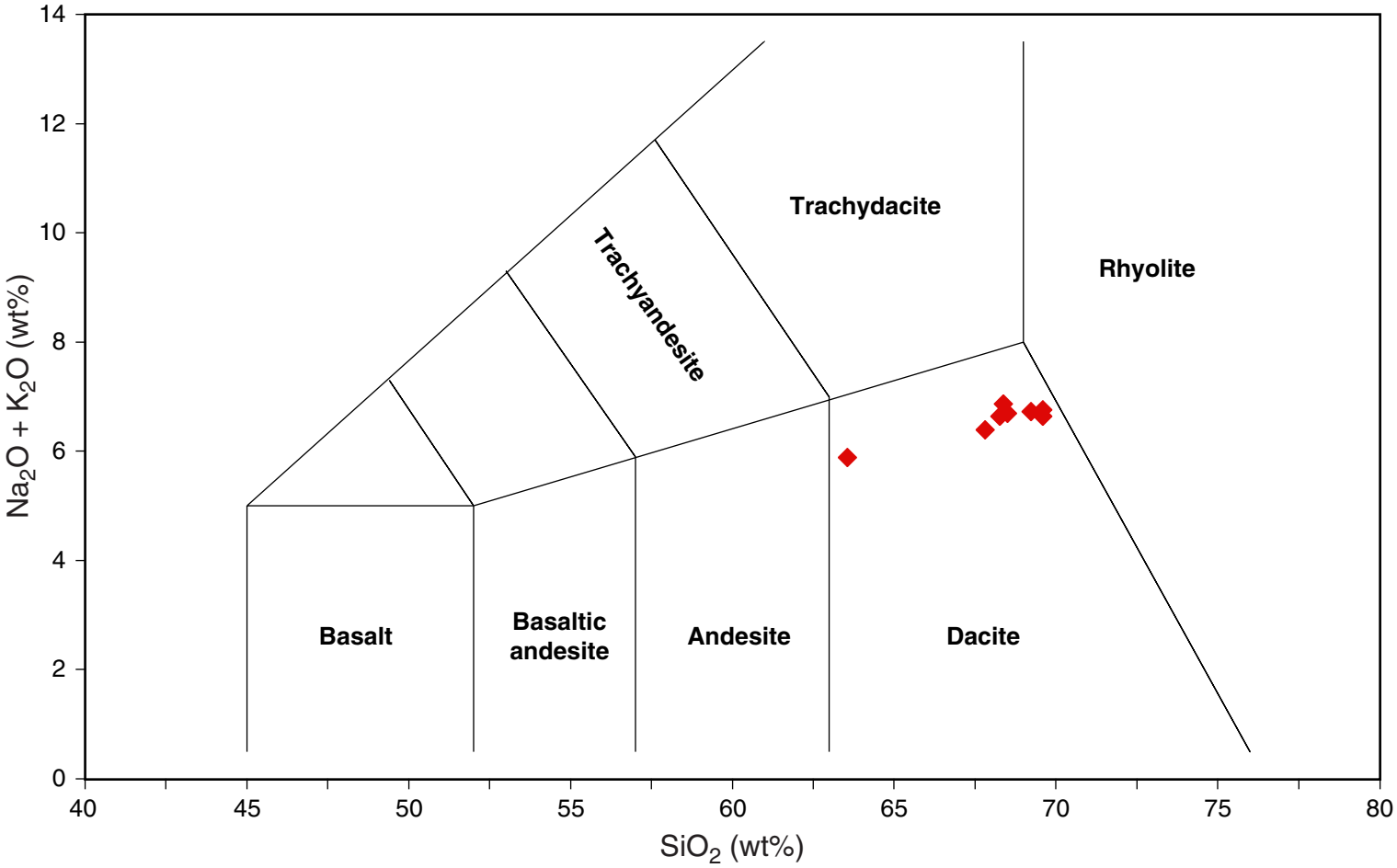

Figure F11. An International Union of Geological Sciences (CIPW norm) classification of fresh volcanic rocks based on quartz, K-feldspar, and plagioclase content. The diagram shows all unaltered volcanic rocks from Hole 1191A, along with single samples from Holes 1188A, 1189A, and 1190C.

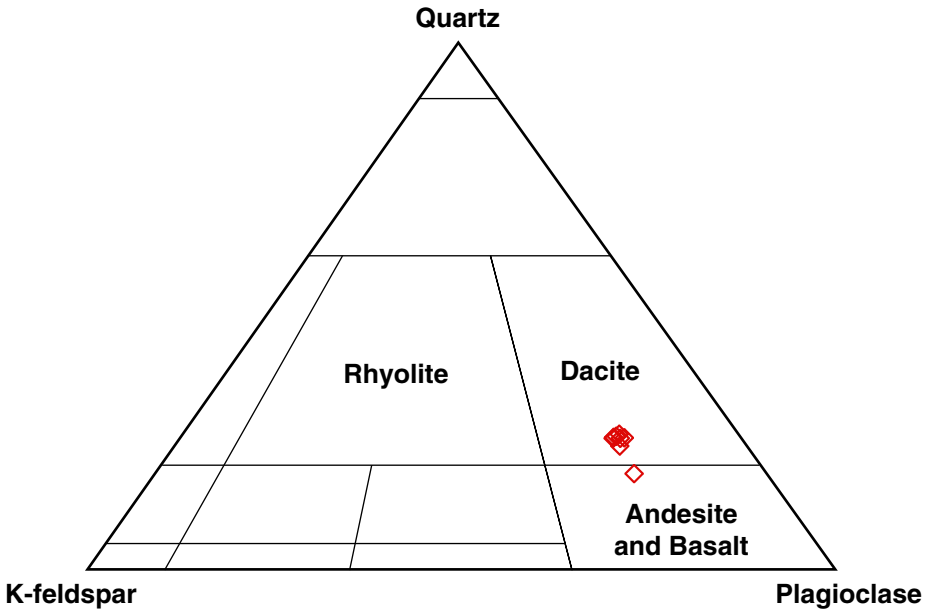

Figure F12. Photomicrographs of dacitic volcanic glass with embedded magnetite showing bacterial habitation (Sample 193-1191A-3R-1, 62–65 cm [15.32 mbsf]). The sample consists mainly of (**A**) brown translucent fragments (see arrows), (**B**) some spherical opaque grains of magnetite (see arrow 1) and lath-shaped plagioclase microlites (see arrow 2) embedded in glass, and (**C**) sparse bacterial populations, including a few colonies (see arrows), which were located on the surfaces of these fragments.

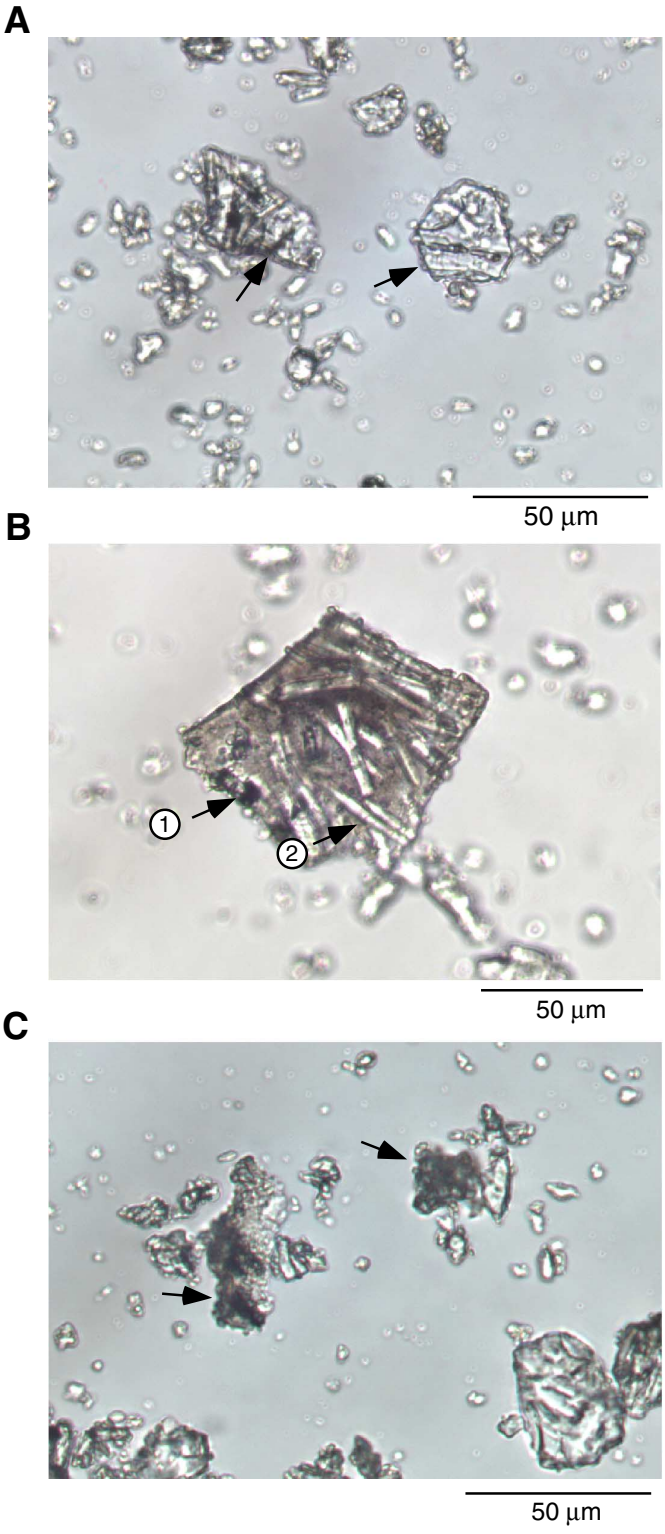

Figure F13. Magnetic susceptibility data from Hole 1191A.

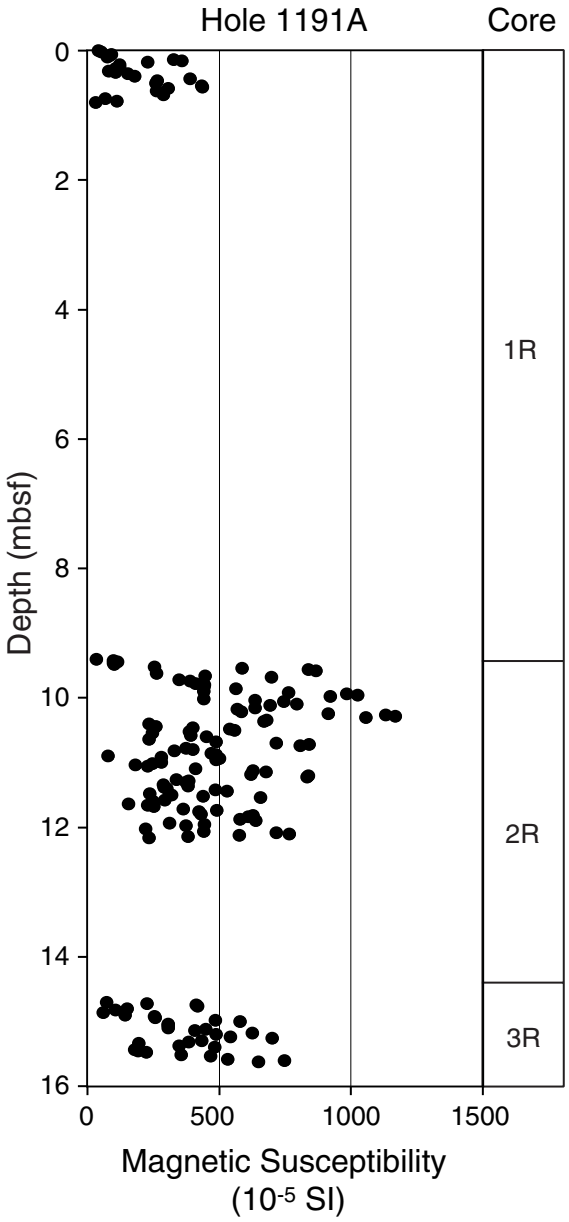

Figure F14. Natural gamma radiation (NGR) data from Hole 1191A.

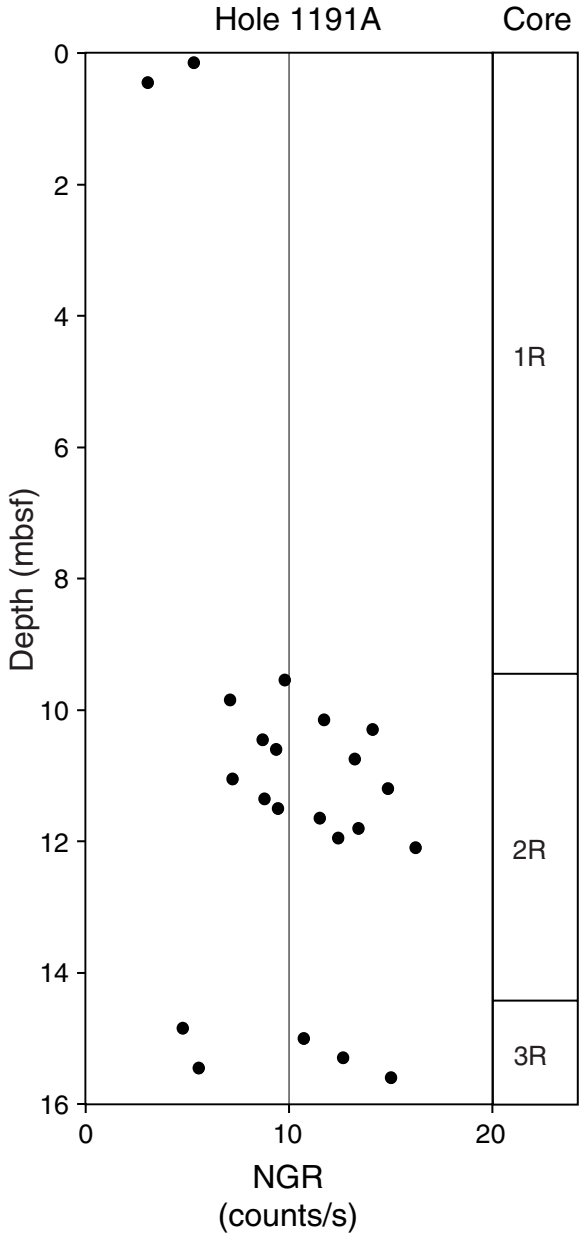

Figure F15. Thermal conductivity data from Hole 1191A.

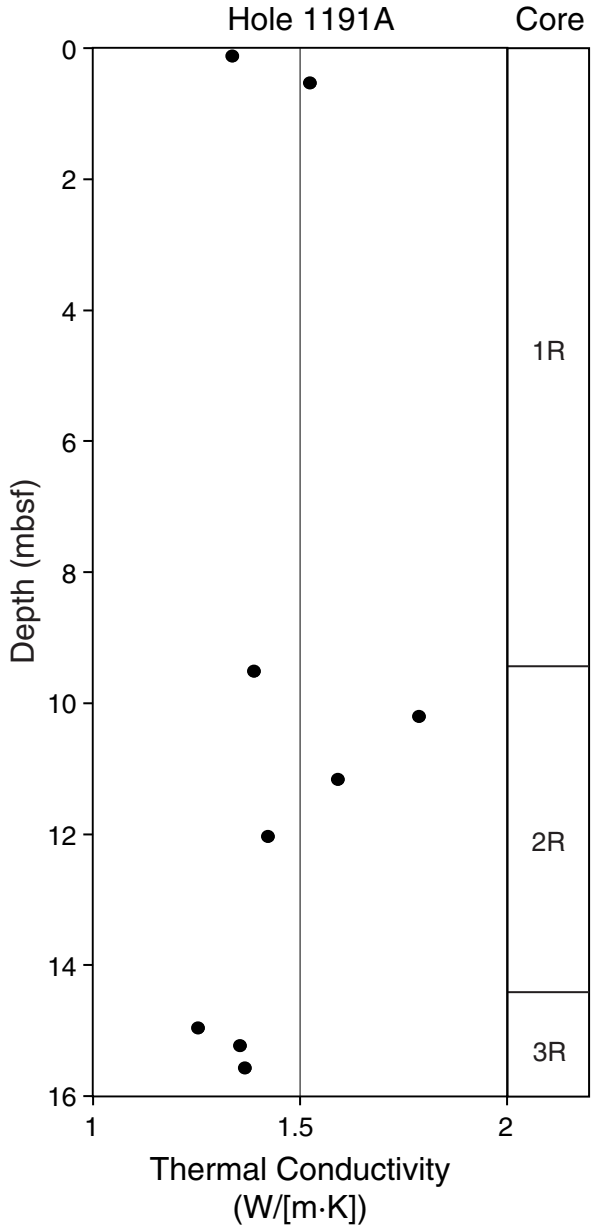

Figure F16. Volume susceptibility vs. depth of archive-half–core and minicore samples from Hole 1191A. Point measurements were taken using the archive multisensor track in manual mode.

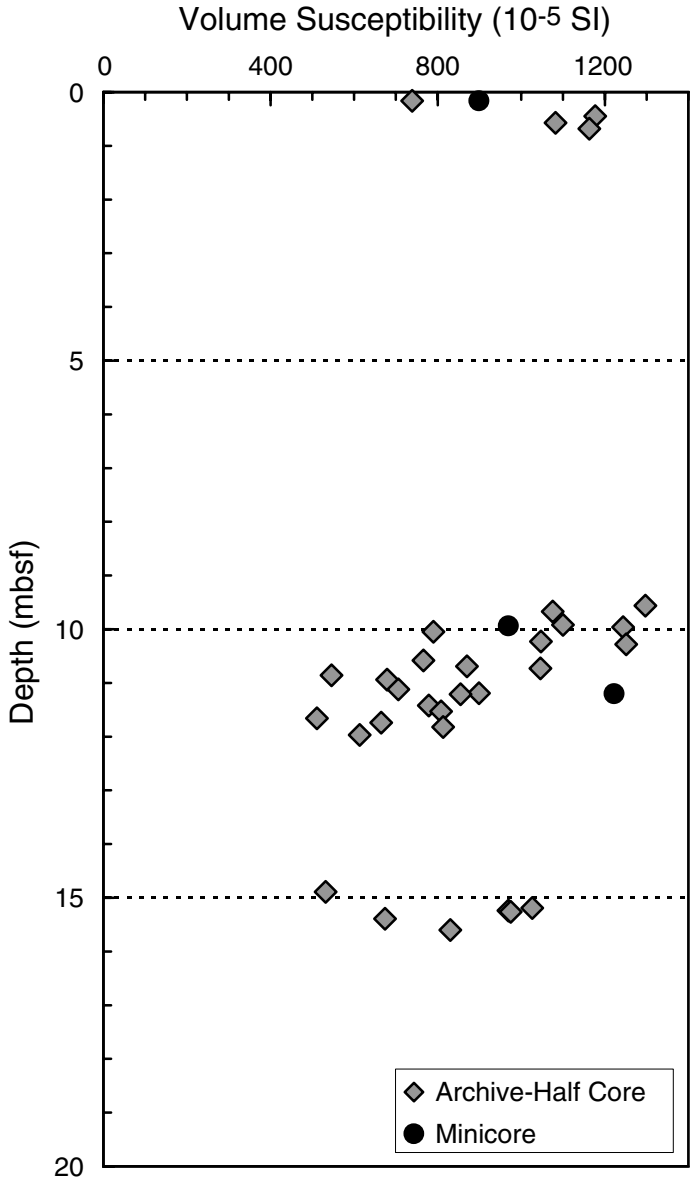

Figure F17. Flinn-type diagram showing the foliation and lineation of the anisotropy of the magnetic susceptibility ellipsoid from Hole 1191A. The minicore samples show very little anisotropy.

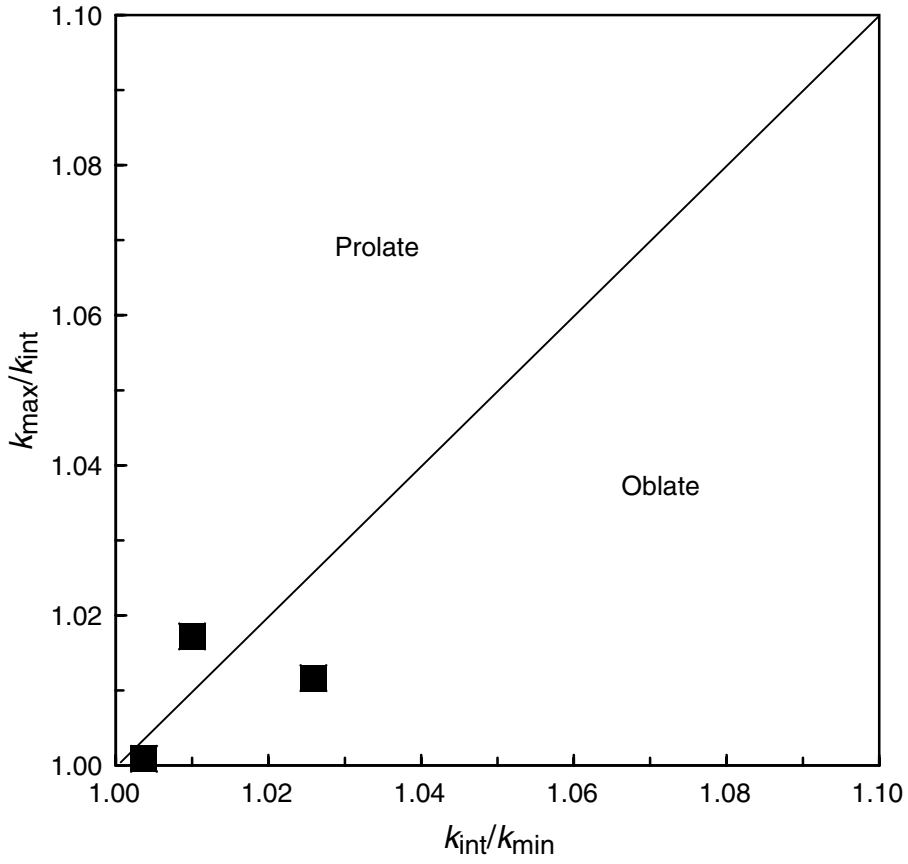

Figure F18. Natural remanent magnetization (NRM) intensity vs. depth of archive-half–core and minicore samples from Hole 1191A. The archive-half data are from Section 193-1191A-2R-1, which had several relatively long pieces. Because this core had gaps and did not fill the core liners, the intensity values are lower than those of the minicore.

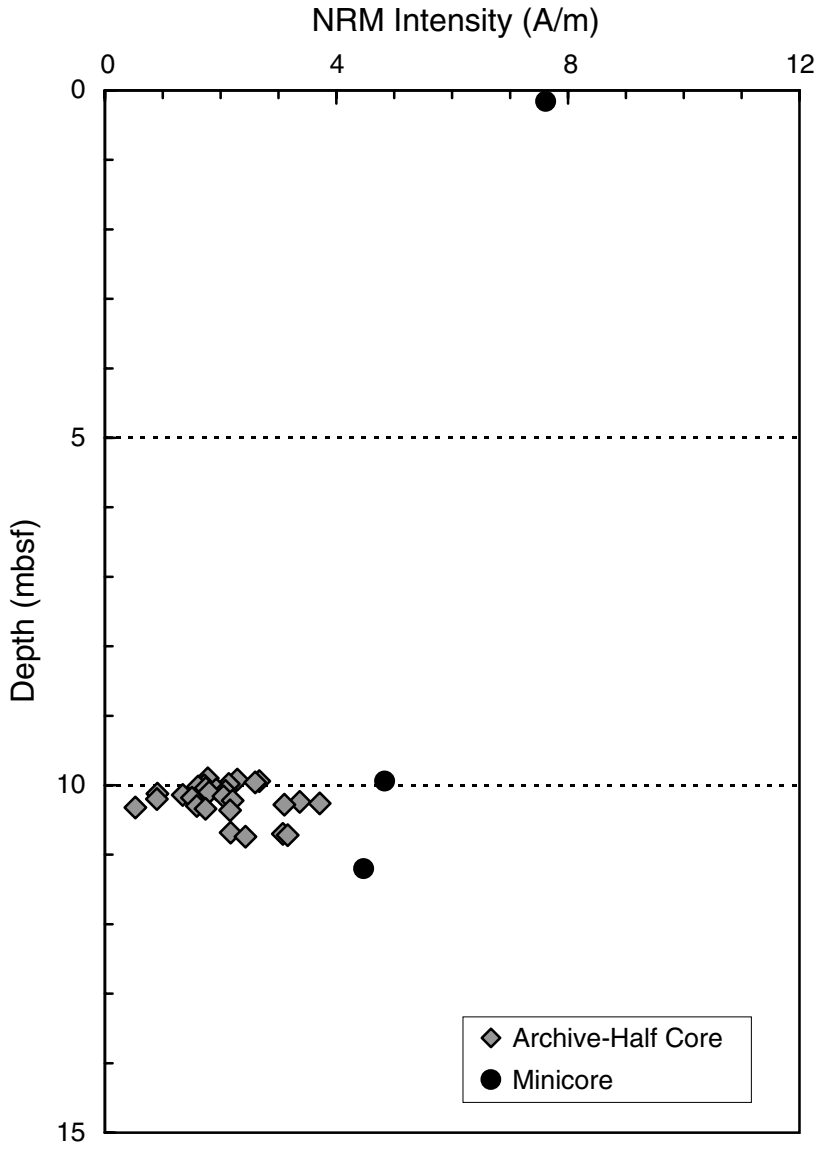

Figure F19. Thermal demagnetization curve of Sample 193-1191A-2R-2, 30 cm. The sample was imparted with an isothermal remanent magnetization (IRM) at an impulse field of 1.1 T.

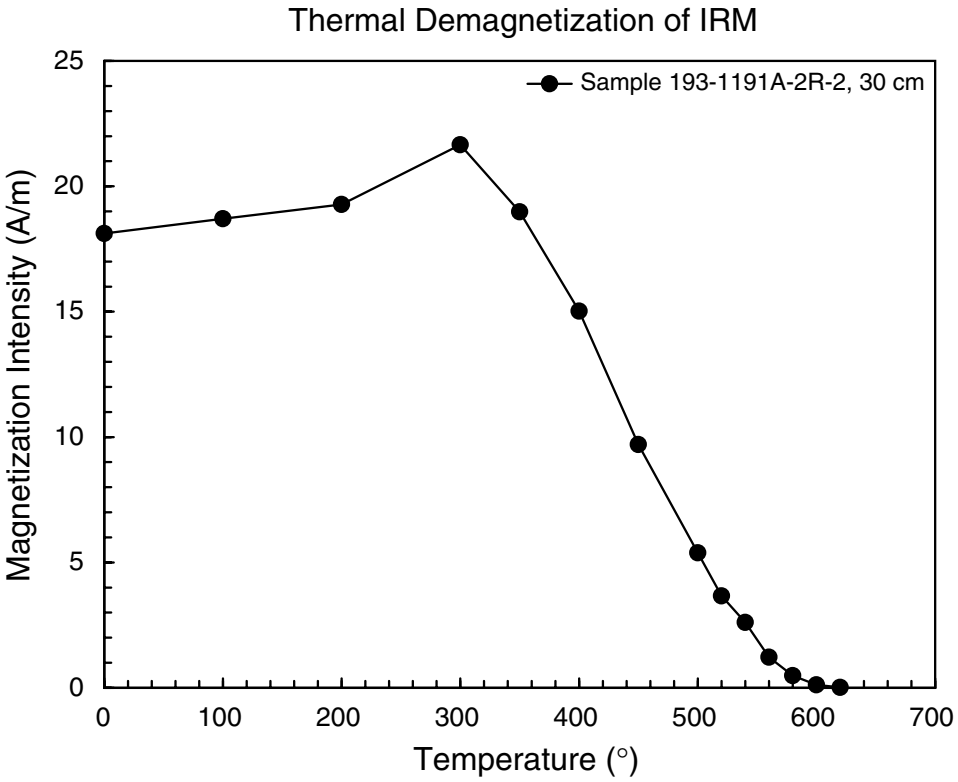

Table T1. Coring summary, Site 1191.

Hole 1191A
Latitude: 03°43.6083′N
Longitude: 151°40.3376′E
Time on site (hr): 45 (1400 hr, 27 Nov 2000–1100 hr, 29 Nov 2000)
Time on hole (hr): 45 (1400 hr, 27 Nov 2000–1100 hr, 29 Nov 2000)
Seafloor (drill pipe measurement from rig floor, mbrf): 1705.0
Distance between rig floor and sea level (m): 10.9
Water depth (drill pipe measurement from sea level, m): 1694.1
Total depth (from rig floor, mbrf): 1725.1
Total penetration (mbsf): 20.1
Total length of cored section (m): 20.1
Total core recovered (m): 3.36
Core recovery (%): 16.72
Total number of cores: 3

Core	Date (Nov 2000)	Time (local)	Top depth (mbsf)	Length (m)		Recovery (%)
				Cored	Recovered	
193-1191A-						
1R	28	0325	0.0	9.4	0.56	6.0
2R	28	0850	9.4	5.3	2.20	41.5
3R	28	1245	14.7	5.4	0.60	11.1

Table T2. Lithology and alteration of Unit 1, Site 1191.

Core, section (Piece)	Curated depth (mbsf) Top	Base	Curated length (m)	Lithology	Alteration
193-1191A-					
1R-1 (1-15)	0.00	0.80	0.80	Fresh to moderately altered aphyric moderately vesicular volcanic rock.	Alteration generally slight. Vesicle fill of zeolites and silica + sulfide. Slight silicification of the groundmass gives the rock a slighty bleached appearance in places. Minor Fe-Oxide staining on some fracture surfaces and vesicles. Sulfide (marcasite and pyrite) veins are common.
2R-1 (1-20)	9.40	10.89	1.49		
2R-2 (1-19)	10.89	12.15	1.26		
3R-1 (1-14)	14.70	15.57	0.87		

Table T3. Results of point counts on volcanic rock thin sections, Site 1191.

Core, section, interval (cm)	Unit	Rock type	Number of points	Groundmass (%)	Vesicles (%)	Phenocrysts (%)		
						Plagioclase	Clinopyroxene	Opaques
193-1191A-								
1R-1 (Piece 2, 5-7)	1	Rhyodacite	650	91.3	8.6	0.0	0.0	0.0
2R-1 (Piece 7, 42-46)	1	Rhyodacite	750	86.2	13.1	0.2	0.1	0.1
2R-2 (Piece 16, 103-106)	1	Rhyodacite	700	90.6	9.3	0.0	0.0	0.0
3R-1 (Piece 1, 4-7)	1	Rhyodacite	750	87.7	12.0	0.2	0.0	0.0
3R-1 (Piece 4, 18-21)	1	Rhyodacite	750	91.7	8.1	0.0	0.1	0.0
3R-1 (Piece 9, 51-54)	1	Rhyodacite	750	85.3	14.6	0.0	0.0	0.0

Note: Point counts were measured using a rectangular grid with a = 0.667 mm and b = 0.8 mm.

Table T4. Minerals identified by XRD analysis, Site 1191.

Core, section, interval (cm)	Unit	Description	XRD identification: major (minor, "trace") minerals*
193-1191A-			
2R-1, 32-36	1	Slightly altered, aphyric, moderately vesicular rhyodacite	Opaline silica (plagioclase, marcasite, pyrite)
3R-1, 18-21	1	Slightly altered, aphyric, moderately vesicular rhyodacite	Opaline silica, plagioclase (cristobalite)
3R-1, 53-54	1	Slightly altered, aphyric, moderately vesicular rhyodacite	Plagioclase, cristobalite ("spinel, ?magnetite")

Notes: XRD = X-ray diffraction. * = the terms major, minor, and trace are applied to XRD analyses as explained in "**Hydrothermal Alteration,**" p. 8, in the "Explanatory Notes" chapter and do not imply quantitative abundances.

Table T5. Major element oxides with selected trace elements, Hole 1191A.

Core, section: 193-1191A-:	1R-1	2R-1	3R-1	3R-1	3R-1
Interval (cm):	5-7	42-45	4-7	18-21	51-54
Curated depth (mbsf):	0.05	9.82	14.47	14.88	15.21
Rock type:	Dacite	Dacite	Dacite	Dacite	Dacite
Alteration style:	Fresh	Fresh	Fresh	Fresh	Fresh
Ignited rock powder composition:					
Major element oxide (wt%):					
SiO_2	69.24	68.67	70.48	70.11	70.48
TiO_2	0.57	0.58	0.59	0.58	0.59
Al_2O_3	14.17	13.97	14.16	14.30	14.40
Fe_2O_3	4.77	4.54	4.80	4.78	4.59
MnO	0.14	0.12	0.12	0.14	0.13
MgO	0.87	0.86	0.89	0.87	0.89
CaO	3.00	3.00	2.94	2.97	2.98
Na_2O	5.19	4.82	5.02	5.06	5.16
K_2O	1.77	1.66	1.71	1.74	1.68
P_2O_5	0.13	0.14	0.14	0.13	0.14
Total (wt%):	99.84	98.35	100.86	100.69	101.05
LOI (wt%):	1.25	0.02	0.15	1.25	1.13
Trace element (ppm):					
Zr	133	138	138	136	137
Y	37	37	36	37	38
Sr	281	274	283	276	281
Zn	108	73	72	102	82
Cu	32	70	24	37	31
Ba	345	344	349	350	353
Whole-rock composition:					
Major element oxide (wt%):					
SiO_2	68.38	67.81	69.60	69.24	69.60
TiO_2	0.56	0.58	0.58	0.57	0.59
Al_2O_3	13.99	13.79	13.98	14.12	14.22
Fe_2O_3	4.71	4.49	4.74	4.72	4.53
MnO	0.14	0.12	0.12	0.14	0.13
MgO	0.86	0.85	0.88	0.86	0.88
CaO	2.96	2.96	2.91	2.93	2.94
Na_2O	5.13	4.76	4.95	5.00	5.10
K_2O	1.75	1.63	1.69	1.72	1.66
P_2O_5	0.13	0.14	0.14	0.13	0.14
Total S (wt%):	0.04	0.00	0.00	0.02	0.00
Total H_2O^+ (wt%):	1.76	0.07	0.00	1.00	0.99

Note: Major element oxides and selected trace element composition of ignited powders measured by inductively coupled plasma-atomic emission spectroscopy followed by loss on ignition and the whole-rock composition, as well as the total sulfur and water contents as measured by NCS elemental analysis.

Table T6. Total bacterial counts and ATP measurements, Hole 1191A.

Hole, core, section	Depth (mbsf)	Direct count (cells/cm^3)	ATP (pg/cm^3)	Active bacterial cells based on ATP content
193-1191A-				
2R	10.55	1.4 x 10^7	2.8	5.5 x 10^4 cells/cm^3
3R	15.32	5.8 x 10^6	2.3	4.5 x 10^4 cells/cm^3

Note: ATP = adenosine triphosphate.

Table T7. Enrichment cultivation at different culture conditions, Hole 1191A.

Hole, core	Depth (mbsf)	Aerobic cultivation			Anaerobic cultivation		
		4°C	25°C	60°C	25°C	60°C	90°C
193-1191A-							
2R	10.55	+	+	—	+	+	+
3R	15.32	—	+	—	+	+	+

Note: + = growth, — = no growth.

Table T8. Compressional wave velocities, Hole 1191A.

Core, section, interval (cm)	Piece	Depth (mbsf)	Velocity (m/s)	Sil/Cl (%)	Vesicles (%)	Alteration	Comments
193-1191A-							
1R-1, 16	2	0.16	5041.0	1	0	Sl	Some zeolites in vesicles.
2R-1, 54	8	9.94	5597.7	10	Tr	Sl	Submillimeter vesicles that are partly filled with silica.

Notes: Sil/Cl = silica/clay. Tr = trace. Sl = slight.

Table T9. Index properties, Hole 1191A.

Core, section, interval (cm)	Piece	Type	Depth (mbsf)	Bulk water content (%)	Density (g/cm^3)			Porosity (%)	Void ratio
					Bulk	Dry	Solid		
193-1191A-									
1R-1, 15-17	3	Minicore	0.15	5.10	2.33	2.21	2.50	11.50	0.13
2R-1, 53-55	8	Minicore	9.93	3.00	2.45	2.37	2.56	7.10	0.08
2R-2, 29-31	5	Minicore	11.19	3.80	2.46	2.36	2.60	9.00	0.10

Table T10. Grain density of powders analyzed by inductively coupled plasma–atomic emission spectroscopy, Hole 1191A.

Core, section, interval (cm)	Depth (mbsf)	Grain density (g/cm^3)
193-1191A-		
1R-1, 5-7	0.05	1.75
2R-1, 42-46	9.82	2.73
3R-1, 4-7	14.47	2.56
3R-1, 18-21	14.88	3.82
3R-1, 51-59	15.21	3.54

Table T11. Magnetic property values for minicores, Hole 1191A.

Number	Core, section, interval (cm)	Depth (mbsf)	Vertically oriented	Volume (cm^3)	NRM (mA/m)	Susceptibility (10^{-5} SI unit)	Koenigsberger ratio	Stable declination (°)	Stable inclination (°)	Brief description
	193-1191A-									
1	1R-1, 16	0.16	Yes	13.6	7618	899	292	91	–19	Black, vesicular, rhyodacite, hard
2	2R-1, 54	9.94	Yes	13.1	4834	969	172	71	–14	Black, vesicular, rhyodacite, hard
3	2R-2, 30	11.20	Yes	13.6	4472	1222	126	144	–17	Black, vesicular, rhyodacite, hard

Note: NRM = natural remanent magnetization.

Table T12. Anisotropy of magnetic susceptibility values for the normalized principal susceptibility values and directions, Hole 1191A.

Core, section, interval (cm)	Depth (mbsf)	k (10^{-5} SI unit)	k_{max} Magnitude	k_{max} Declination (°)	k_{max} Inclination (°)	k_{int} Magnitude	k_{int} Declination (°)	k_{int} Inclination (°)	k_{min} Magnitude	k_{min} Declination (°)	k_{min} Inclination (°)	Error (10^{-5} SI unit)	P
193-1191A-													
1R-1, 16	0.16	899	1.0163	360	0.6	1.0046	89.9	39.2	0.9792	270.0	50.7	3.1	1.0378
2R-1, 54	9.94	969	1.0147	216	37.2	0.9976	332.0	30.5	0.9877	89.9	37.8	2.9	1.0274
2R-2, 30	11.20	1222	1.0018	103	8.1	1.0009	360.0	58.2	0.9973	198.0	30.4	2.8	1.0046

Notes: Axes of susceptibility ellipsoid: k = volume susceptibility, k_{max} = maximum, k_{int} = intermediate, and k_{min} = minimum. P = degree of magnetic anisotropy.

Table T13. Magnetic properties for minicores after successive alternating field demagnetization, Hole 1191A.

Core, section, interval (cm)	Depth (mbsf)	Demagnetization level (mT)	Declination (°)	Inclination (°)	Intensity (mA/m)
193-1191A-					
1R-1, 16	0.16	0	93	–14	7.618
		10	91	–19	7.451
		15	90	–24	7.280
		20	91	–25	7.112
		25	90	–24	6.958
		30	91	–27	6.791
		40	91	–29	6.508
		50	91	–29	6.113
		60	92	–29	5.688
		80	92	–30	4.757
2R-1, 54	9.94	0	74	–11	4.834
		10	71	–14	4.414
		15	71	–15	3.927
		20	71	–15	3.503
		25	71	–14	3.165
		30	72	–14	2.911
		40	72	–14	2.607
		50	72	–14	2.319
		60	73	–14	2.092
		80	73	–15	1.695
2R-2, 30	11.20	0	146	–13	4.472
		10	144	–17	3.863
		15	144	–18	3.329
		20	145	–19	2.901
		25	146	–20	2.605
		30	147	–22	2.414
		40	148	–22	2.187
		50	148	–23	1.953
		60	148	–23	1.736
		80	149	–23	1.316